arXiv:1402.1851v1 [hep-lat] 8 Feb 2014

Asymptotic safety on the lattice: The Nonlinear O(N) Sigma Model

Björn H. Wellegehausen*
Institut für Theoretische Physik, Justus-Liebig-Universität Giessen, 35392 Giessen, Germany and
Theoretisch-Physikalisches Institut, Friedrich-Schiller-Universität Jena, 07743 Jena, Germany

Daniel Körner† and Andreas Wipf‡
Theoretisch-Physikalisches Institut, Friedrich-Schiller-Universität Jena, 07743 Jena, Germany

We study the non-perturbative renormalization group flow of the nonlinear O(N) sigma model in two and three spacetime dimensions using a scheme that combines an effective local Hybrid Monte Carlo update routine, blockspin transformations and a Monte Carlo demon method. In two dimensions our results verify perturbative renormalizability. In three dimensions, we determine the flow diagram of the theory for various N and different truncations and find a non-trivial fixed point, which indicates non-perturbative renormalizability. It is related to the well-studied phase transition of the O(N) universality class and characterizes the continuum physics of the model. We compare the obtained renormalization group flows with recent investigations by means of the Functional Renormalization Group.

PACS numbers: 11.15.-q, 11.15.Ha, 12.38.Aw

I. INTRODUCTION

The renormalization of coupling parameters due to quantum fluctuations is a characteristic feature of any quantum field theory and many different methods have been developed to study this interesting property. While most of these methods rely on a perturbative treatment of the theories, the investigation of strongly coupled or strongly correlated systems without small expansion parameter, like e.g. the theory of strong interaction, requires a non-perturbative approach. One non-perturbative and very flexible method is the *Functional Renormalization Group* (FRG) introduced by K. Wilson [1]. In a particularly useful implementation of the functional renormalization group, one studies the flow of the effective average action Γ_k w.r.t. the momentum scale k, which interpolates between the bare action at the UV-cutoff Λ, and the full effective action in the IR, $\Gamma_{k\to 0} = \Gamma$ [2]. With the help of this powerful non-perturbative approach one can explore theories which are non-renormalizable in perturbation theory, i.e. in the vicinity of a Gaußian fixed point, but are renormalizable in a non-perturbative setting. In such asymptotically save theories the running of the couplings in the UV is controlled by a non-trivial fixed point with a finite number of relevant directions. The most important theory where this so-called *asymptotic safety scenario* of Weinberg [3, 4] could be realized is general relativity where at present all results suggest that there exists a non-trivial UV fixed point [5–7].

Here we employ an alternative and efficient non-perturbative approach, based on numerical simulations, to study global flow diagrams of field theories. We apply the technique to spot non-trivial fixed points and to determine their properties. In order to extract the renormalization of the couplings from lattice computations, different methods are used to define the running coupling such as the renormalized correlation functions or the Schwinger functional [8]. In an alternative recent approach one tries to directly integrate out momentum shells on the lattice by using Fourier Monte Carlo simulation [9]. In the present work we make use of the well-known *Monte Carlo Renormalization Group* method (MCRG) [10–13]. It is based on the idea of blockspin transformations and can be applied to theories with fermionic or gauge fields [14]. By applying successive blockspin transformations, real-space RG-transformations are performed and a renormalization trajectory is calculated. However, since every RG step typically reduces the linear extent of the lattice by a factor of $b = 2$, exponentially large lattices are needed in order to obtain sufficiently long trajectories that get close enough to the fixed point regime [15]. Even worse, a standard method to determine the effective couplings relies on the matching of correlation functions on the initial and blocked lattices and requires expensive scanning runs for the parameters of the bare action at the largest lattice used [16]. In order to circumvent these problems we employ the *demon method* [17–19] which allows us to efficiently compute RG trajectories at a fixed lattice volume.

In the present work we apply the MCRG method in combination with the demon method to calculate the global flow diagram of the ubiquitous nonlinear O(N) sigma models (NLSM) which are of interest both in condensed matter physics [20] and in particle physics [21]. Here they serve as toy models to test and develop RG methods for models of quantum gravity. Both classes of theories share relevant properties. Whereas in two dimensions the nonlinear O(N) models are perturbatively renormalizable and asymptotically free this feature is lost in higher dimensions. But then the small-ϵ and $1/N$-expansions both point to the the existence of non-trivial fixed points in these models [22–25]. Their existence is further supported by FRG calculations based on a one-parameter truncation of the effective action [26] and higher-order truncations [27] and we will compare our computations with these more recent results.

The article is structured as follows: In Sec. II we discuss general properties of nonlinear O(N) models and in Sec. III we de-

* Bjoern.Wellegehausen@uni-jena.de
† Daniel.Koerner@uni-jena.de
‡ Wipf@tpi.uni-jena.de

scribe both the MCRG and the demon method. We carefully discuss the truncation of the effective action and the optimization of the MCRG method. In Sec. IV we apply the method to the asymptotically free two-dimensional sigma model and recover the expected flow of couplings and fixed point structure. In Sec. V we study the flow diagram of the three dimensional O(3) model. We begin with a simple one-parameter truncation and then include operators of higher order in the derivatives. We also compute the critical exponents and compare the obtained values with known results. In Sec. VI we continue with the flow diagrams and critical exponents of O(N) models for different values of N and study the large-N limit. Our general conclusion is contained in Sec. VII. Preliminary results of this work have been reported in the proceedings [28].

II. THE O(N) NONLINEAR SIGMA MODEL IN d DIMENSIONS

We recall the Euclidean action of the nonlinear O(N) model with the sphere as target space,

$$S_\sigma = \frac{1}{2g^2}\int d^dx\, \partial_\mu \boldsymbol{\phi}\cdot\partial^\mu\boldsymbol{\phi}, \tag{1}$$

where $\boldsymbol{\phi}$ is a N-component scalar field that satisfies the constraint $\boldsymbol{\phi}\cdot\boldsymbol{\phi}=1$. The coupling g has mass dimension

$$[g] = \frac{2-d}{2}. \tag{2}$$

In two spacetime dimensions the global O(N) symmetry cannot be broken. At strong coupling the theory is asymptotically free and the RG flow is dominated by a fixed point at infinite coupling, which corresponds to a Gaußian fixed point for the inverse coupling. Thus, the model is perturbatively renormalizable. This is not surprising since in two dimensions the coupling is dimensionless. In higher dimensions the coupling has negative mass dimension and perturbative renormalizability is lost. However, lattice simulations with the discretized action

$$S = \frac{1}{2g^2}\sum_{x,\mu}\boldsymbol{\phi}_x\boldsymbol{\phi}_{x+\hat{\mu}} \tag{3}$$

reveal a critical point that separates a O(N) symmetric phase from a broken phase by a second-order phase transition. In the broken phase there are $N-1$ Goldstone bosons corresponding to the directions tangential to a sphere in target space. In order to recover the continuum field theory one may use this critical behavior to define the continuum limit of the discrete lattice model. Much effort went into studying the properties of the model near criticality and in particular in calculating its critical exponents. Thus, a large number of results are available, both from numerical high-precision Monte Carlo methods as well as analytical calculations using the high-temperature expansion or renormalization group method. Even experimental data from condensed matter physics are available, see for example [11, 15, 16, 20, 26, 29–32].

We are particularly interested in the flow diagram of the three-dimensional model that is conjectured to show a non-trivial UV fixed point, a necessary requirement for the asymptotic safety scenario to be at work.

III. MONTE CARLO RENORMALIZATION GROUP

We will study the O(N) lattice model at zero temperature, i.e. on a lattice with equal temporal and spatial extent L. The physical volume is hence $V = L_{\rm phys}^d = (aL)^d$, where a denotes the lattice spacing. In Monte Carlo simulations a UV-cutoff at an energy $\Lambda = \pi/a$ is introduced naturally and the lattice size $L_{\rm phys}$ serves as IR-cutoff at a lower energy $\lambda = \pi/L_{\rm phys}$. On the lattice one may calculate the n-point functions

$$\langle\phi_{x_1}\dots\phi_{x_n}\rangle = \frac{\int\mathcal{D}\phi\,\phi_{x_1}\dots\phi_{x_n}\,\exp(-\Gamma_\Lambda[\phi])}{\int\mathcal{D}\,\phi\exp(-\Gamma_\Lambda[\phi])} \tag{4}$$

from which one extracts all physical quantities like e.g. particle masses. Thereby all quantum fluctuations with scales between the upper and lower cutoff are taken into account. The physics at the IR-cutoff is fixed by choosing a lattice extent L and coupling constants g_i of the microscopic (bare) action at the UV-cutoff. An RG transformation $R_{\Lambda\mapsto\Lambda'}$ relates the parameter set $\{g_i\}$ at the high energy scale Λ to a parameter set $\{g_i'\}$ at lower energy scale Λ',

$$\{g_i\}(\Lambda)\longmapsto\{g_i'\}(\Lambda') = R_{\Lambda\mapsto\Lambda'}\left(\{g_i\}\right). \tag{5}$$

Thereby the physics, i.e. the n-point functions at the lower cutoff λ, remain unchanged. An important property of any such RG transformation is that it does not depend on the details of the flow in coupling space. In particular the transformation must obey the semigroup properties

$$R_{\Lambda\mapsto\Lambda'} = R_{\Lambda\mapsto\Lambda''}\circ R_{\Lambda''\mapsto\Lambda'},\quad R_{\Lambda\mapsto\Lambda}=1, \tag{6}$$

where $\Lambda>\Lambda''>\Lambda'$. This is depicted in Fig. 1. The infinitesimal change of the couplings is described by the β-functions

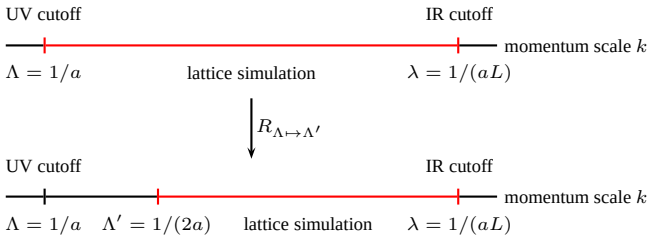

FIG. 1. Sketch of the MCRG method

$$\beta_i(g) = \partial_t g_i\,,\quad t=\ln\Lambda. \tag{7}$$

The critical exponents $\{\theta_i\}$ of the theory are defined as the negative eigenvalues of the stability matrix

$$S_{ij} = \left.\frac{\partial\beta_i}{\partial g_j}\right|_{g=g^*} \tag{8}$$

at the fixed points g^* of the theory defined by $\beta_i(g^*)=0$. Positive critical exponents belong to relevant direction, neg-

ative exponents to irrelevant directions and vanishing exponents to marginal directions, i.e.

$$\begin{aligned} \theta_i > 0 \quad & \textit{relevant} \text{ direction}, \\ \theta_i < 0 \quad & \textit{irrelevant} \text{ direction}, \\ \theta_i = 0 \quad & \textit{marginal} \text{ direction}. \end{aligned} \tag{9}$$

By comparing with the scaling of singular thermodynamic observables near a critical point, one obtains relations between the thermodynamic critical exponents and the eigenvalues of the stability matrix, for example $\nu = \theta_r^{-1}$ for the critical exponent of the correlation length ν and the eigenvalue θ_r of the related relevant direction.
In our setup, an RG transformation consists of the two steps illustrated in Fig. 2:

1. A blockspin transformation applied to an ensemble with fixed couplings $\{g_i\}$. For the blockspin transformation the semigroup properties are fulfilled.

2. The demon method to *measure* the effective couplings $\{g_i'\}$ on the blocked lattice. Since this method can only be applied to a truncated effective action the semigroup property of the composite transformation is violated in this step.

In the following we will discuss both steps in more detail.

A. Blockspin transformation

A blockspin transformation with scale parameter b relates a field configuration $\{\phi_x\}$ on the fine lattice (N, a) to an averaged configuration $\{\phi_x'\}$ on the coarser lattice $(N' = N/b, a' = ba)$ [33]. The IR-cutoff does not change and the blocked and initial configurations describe the same macroscopic physics. In contrast, the UV-cutoff $\Lambda \to \Lambda' = \Lambda/b$ is lowered and the effective parameters $\{g_i'\}$ defined at the new cutoff Λ' incorporate the effects of all quantum fluctuations with scales between Λ and Λ'. A numerical simulation on the coarse lattice with couplings $\{g_i'\}$ yields the same distribution of averaged fields $\{\phi_x'\}$ as obtained from a simulation at the fine lattice with $\{g_i\}$. Each set of parameters defines a point in theory space and they are connected by an RG trajectory.
Here we employ a blockspin transformation where one draws the averaged fields according to a normalized probability distribution,

$$\mathcal{P}(\phi_x') \propto \exp\big(C(g)\,\phi_x' \cdot R(\{\phi_x\})\big), \tag{10}$$

where $R(\{\phi_x\}) = \sum_{y\in\square_x} \phi_y$ is the sum over all degrees of freedom within a hypercube of the fine lattice. In our computations we choose the smallest cube of size $b^d = 2^d$. The positive function $C(g)$ determines how strongly the blocked fields may fluctuate away from the original degrees of freedom. We shall use a function which minimizes the systematic errors induced by the unavoidable truncation of the effective action. A detailed discussion is found in Sec. III D.

B. The demon method

With the microcanonical demon method [17] one can calculate the couplings in an effective action $S = \sum_i g_i S_i$ such that the corresponding distribution is close to a given ensemble of lattice configurations. Hence, given a partition function

$$Z(\beta) = \int \mathcal{D}\omega \exp\{-\beta H(\omega)\} \tag{11}$$

one introduces an additional degree of freedom E_D, the *demon energy*, with the combined partition function

$$Z_{\mathrm{D}}(\beta) = \int \mathcal{D}\omega \int dE_D \, \exp\{-\beta H(\omega) - \beta E_D\} \tag{12}$$

of the canonical demon ensemble. The expectation value of the demon energy can be calculated in a simulation of the microcanonical ensemble,

$$Z_{\mathrm{MCD}} = \int \mathcal{D}\omega \int dE_D \, \delta\left(H + E_D - E_0\right), \tag{13}$$

and is related to the inverse temperature β,

$$\langle E_D \rangle = \langle E_D \rangle\,(\beta), \tag{14}$$

thus allowing to *measure* the inverse temperature β corresponding to the combined ensemble. This method can be generalized to more than one temperature or coupling constant, i.e.

$$Z_{\mathrm{MCD}} = \int \mathcal{D}\omega \prod_i \int dE_D^i \, \delta\left(S^i + E_D^i - E_0^i\right). \tag{15}$$

Constraining the demon energy to $E_D^i \in (-E_m^i, E_m^i)$ yields

$$\left\langle E_D^i \right\rangle_{\mathrm{D}} = \frac{1}{g_i} - \frac{E_m}{\tanh(g_i E_m)} \approx \left\langle E_D^i \right\rangle_{\mathrm{MCD}} \tag{16}$$

where the subscript D denotes the canonical demon ensemble (12) and MCD the microcanonical demon ensemble (13). This equation can be solved by numerical means and is used to extract the coupling constants $\{g_i\}$ from the mean demon energies on the right hand side. In the microcanonical ensemble the total energy is fixed. Since we want to measure the couplings of the blocked ensemble without interference from the demon, we demand that $\left|E_D^i\right| \ll \left|S^i\right|$. Then the algorithm for our MCRG setup reads as follows:

1. Pick a configuration distributed according to the canonical ensemble with action $S = g_1 S_1 + g_2 S_2 + \ldots$ on the fine lattice.

2. Perform a blockspin transformation on this configuration.

3. Use the result as starting configuration for a microcanonical simulation of the combined system (15) and measure the mean demon energies. The starting values for the demon energies are given by the mean demon energies extracted from the previous microcanonical runs.

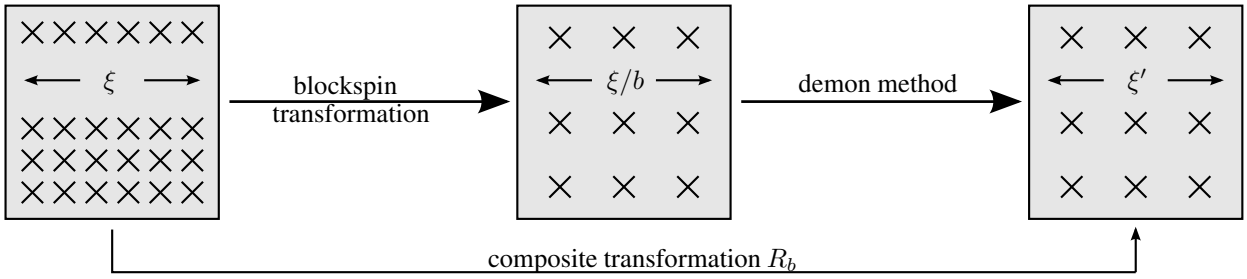

FIG. 2. The composite transformation R_b relates coupling constants on a lattice with correlation length ξ to a coarser lattice with correlation length ξ', which is obtained by using a blockspin transformation and mapping the resulting configurations onto a truncated effective action by the demon method. Simulating the truncated ensemble may not necessarily yield $\xi' = \xi/b$ due to truncation errors.

4. Repeat step one to three until a sufficient number of configurations has been generated.

5. Calculate the couplings g_i' from the mean demon energies.

A comparison of these couplings with the initial ones yields an approximation for the running of the coupling. It reads:

$$\beta_i\,(g) = \partial_t g_i = -a\frac{\partial g_i}{\partial a} = -(g_i' - g_i). \tag{17}$$

Note that the g_i are the dimensionless couplings on the lattice. In order to measure the critical exponents, we introduce a hypercubic grid in coupling space with spacings δg_i and compute the matrix S_{ij},

$$S_{ij}(g) = \frac{\partial \beta_i}{\partial g_j} = \frac{\beta_i(g_j + \delta g_j) - \beta_i(g_j - \delta g_j)}{2\delta g_j}\,. \tag{18}$$

The additional systematic error from discretizing the second derivative can be made arbitrarily small by choosing a finer grid in the space of couplings. Finally we compute the matrix $S_{ij}(g)$ and its eigenvalues $\theta_i(g)$ at couplings in the vicinity of a critical point g^* to obtain the critical exponents and associated thermodynamical critical exponents.

C. Truncated effective action

In general, more and more operators are generated by the repeated application of the blockspin transformations and this yields a trajectory in theory space. Since it is impossible to keep track of all operators we restrict our analysis to an ansatz for the effective action that only includes a finite number of operators. Thereby, the demon method leads to a projection of RG trajectories from general theory space down to modified trajectories in a truncated theory space that only consists of the terms contained in the effective action. Naturally, this procedure introduces additional systematic uncertainties which we will denote as truncation errors. A qualitative understanding of the truncation errors is obtained by comparing different truncations. For this reason, we utilize a systematic derivative expansion of the effective action up to fourth order. In the continuum formulation it is given by

$$S[\boldsymbol{\phi}] = \sum_{i=0}^{3} g_i N S_i[\boldsymbol{\phi}] + \mathcal{O}(\partial^6) \tag{19}$$

with operators

$$S_0 = -\int d^d x\; \boldsymbol{\phi}\cdot\partial_\mu\partial^\mu\boldsymbol{\phi} \tag{20}$$

$$S_1 = \int d^d x\; \boldsymbol{\phi}\cdot(\partial_\mu\partial^\mu)^2\boldsymbol{\phi} \tag{21}$$

$$S_2 = \int d^d x\; (\boldsymbol{\phi}\cdot\partial_\mu\partial^\mu\boldsymbol{\phi})^2 \tag{22}$$

$$S_3 = \int d^d x\; (\boldsymbol{\phi}\cdot\partial_\mu\partial^\nu\boldsymbol{\phi})(\boldsymbol{\phi}\cdot\partial^\mu\partial_\nu\boldsymbol{\phi}). \tag{23}$$

Note that we have introduced an additional factor N in (19) in order to get rid of the leading N dependence of the couplings g. The couplings have mass dimension

$$[g_0] = d-2\,, \quad [g_i] = d-4 \quad \text{for} \quad i = 1,2,3. \tag{24}$$

This is a complete set of the fourth order operators that are compatible with the symmetries of the model. Note that other RG studies (like the one in [27]) employ an alternative parametrization of the effective action. The relation between these two formulations is explained in Appendix A.
Now we discretize the action (19) on a hypercubic lattice,

$$S\big(\{\phi_x\}\big) = \sum_{i=0}^{3} g_i N S_i'\big(\{\phi_x\}\big), \tag{25}$$

where a straightforward discretization of the continuum operators is given by

$$S'_0 = 2\sum_{x,\mu} \Phi_x \cdot \Phi_{x+\mu} - 2dV \tag{26}$$

$$S'_1 = 2\sum_{x,\mu,\nu} \Phi_x \cdot (\Phi_{x+\mu+\nu} + \Phi_{x+\mu-\nu}) - 4d\sum \Phi_x \cdot \Phi_{x+\mu} + 4d^2V \tag{27}$$

$$S'_2 = \sum_{x,\mu,\nu} \{(\Phi_x \cdot \Phi_{x+\mu})(\Phi_x \cdot \Phi_{x+\nu}) + (\Phi_x \cdot \Phi_{x-\mu})(\Phi_x \cdot \Phi_{x-\nu}) + 2(\Phi_x \cdot \Phi_{x+\mu})(\Phi_x \cdot \Phi_{x-\nu})\} - 8d\sum_{x,\mu} \Phi_x \cdot \Phi_{x+\mu} + 4d^2V \tag{28}$$

$$\begin{aligned} S'_3 = &\sum_{x,\mu,\nu} \{(\Phi_x \cdot \Phi_{x+\mu})(\Phi_x \cdot \Phi_{x+\nu}) + (\Phi_x \cdot \Phi_{x-\mu})(\Phi_x \cdot \Phi_{x-\nu}) - 2(\Phi_x \cdot \Phi_{x+\mu})(\Phi_x \cdot \Phi_{x+\nu-\mu}) \\ &- 2(\Phi_x \cdot \Phi_{x-\mu})(\Phi_x \cdot \Phi_{x+\mu-\nu}) + (\Phi_x \cdot \Phi_{x+\nu-\mu})(\Phi_x \cdot \Phi_{x+\mu-\nu}) + 2(\Phi_x \cdot \Phi_{x+\mu-\nu})\} \\ &+2d\sum_{x,\mu} (\Phi_x \cdot \Phi_{x+\mu})(\Phi_x \cdot \Phi_{x-\mu}) - 4d\sum_{x,\mu} \Phi_x \cdot \Phi_{x+\mu} + d^2V. \end{aligned} \tag{29}$$

This set of lattice operators forms a basis of the space of fourth-order derivative operators, but it is not orthogonal in operator space. In order to improve the convergence of the demon method it is useful to reparametrize the action functional in terms of the operators S'_i given by

$$\begin{pmatrix} S'_0 \\ S'_1 \\ S'_2 \\ S'_3 \end{pmatrix} = \begin{pmatrix} 2 & 0 & 0 & 0 \\ -4d & 2 & 0 & 0 \\ -8d & 0 & 1 & 0 \\ -4d & 0 & 0 & 1 \end{pmatrix} \begin{pmatrix} \hat{S}_0 \\ \hat{S}_1 \\ \hat{S}_2 \\ \hat{S}_3 \end{pmatrix} + \begin{pmatrix} -2dV \\ 4d^2V \\ 4d^2V \\ d^2V \end{pmatrix}. \tag{30}$$

For simplicity we drop the hat over lattice quantities in the following.

D. Optimized blockspin transformation

In a lattice simulation we have access to observables (like e.g. the masses) which receive contributions from *all possible* lattice operators. This information, which is in part lost if one uses a truncated effective action, allows us to extend our analysis of truncation errors. The macro-physics is completely determined by the correlation functions and hence must agree for the original and blocked ensemble in Figure 2, since the blockspin transformation does not change the IR physics. Applying the demon method leads to a truncated ensemble which is defined by the effective action. In general, the correlation functions of the blocked and truncated ensemble do not coincide. This discrepancy is solely due to the truncation of the effective action. In addition to the simulation of the blocked ensemble, we also simulate the truncated ensemble in order to measure the difference in the correlation functions and thus quantify the systematic truncation errors directly.

We reduce this difference by adjusting the blockspin transformation. The location of the renormalized trajectory depends on the chosen renormalization scheme [10] and we aim at constructing a scheme for which the renormalized trajectory is closest to our truncated effective action. More accurately, we have used the improved blockspin transformation (10) and tuned the free parameter C. In general, the optimal value depends on the coupling constants, lattice size, target space and number of RG steps. Only in the ideal world without truncation we expect our results to be independent of the RG scheme and thus the optimization constant C.

In order to tune the constant C in the improved blockspin transformation, we compare the correlation lengths extracted from the two-point-functions on the fine and coarse lattice and ignore all other correlation functions. Blockspin transformations reduce the lattice correlation length ξ exactly by a factor b and thus we demand the correlation length ξ' in the truncated ensemble to be equal to ξ/b in order to minimize truncation errors. For simplicity, we allow the optimization constant to depend linearly on the couplings,

$$C(g) = \sum_i c_i g_i\,, \quad c_i = \text{const.}\,. \tag{31}$$

It is clear from the structure of (10) that the choice $C = 0$ leads to a complete loss of information and thus results in a trivial flow diagram. In most of the following computations we find that it is sufficient to tune only the first parameter c_0 since in the vicinity of the non-Gaußian fixed points the corresponding couplings g_i are small compared to g_0. Nevertheless, a small but non-vanishing value for the other c_i is necessary to improve the flow in the vicinity of the Gaußian fixed point. Finally we note that the lattice itself together with the blockspin transformation acts as the regulator function in FRG calculations. Tuning the ratio of correlation functions to the optimal ratio corresponds to the choice of an optimal regulator in the FRG framework. Roughly speaking it minimizes the *flow time* (RG steps) from the UV to the IR.

IV. THE RG FLOW IN TWO DIMENSIONS

In order to test and optimize our method, we reproduce the beta function for the two dimensional O(N) sigma model,

which has already been computed using the MCRG matching method for $N = 3$ [16] and $N \to \infty$ [10, 34]. The coupling constant g_0 of the standard action S_0 is dimensionless and the theory is thus perturbatively renormalizable. From asymptotic freedom we expect that the flow diagram contains two trivial fixed points, one in the IR at vanishing coupling and the other in the UV at infinite coupling, i.e. vanishing inverse coupling [15]. However for numerical simulations only finite lattices are accessible and the theory possesses a transition from a symmetric regime at low coupling (large physical volume) to an ordered regime at strong coupling (small physical volume). The expectation value of the scalar field,

$$\varphi = \left\langle \left| \frac{1}{V} \sum_x \Phi_x \right| \right\rangle, \tag{32}$$

is shown in Fig. 3 as a function of the coupling for different lattice sizes. With increasing volume the transition shifts to

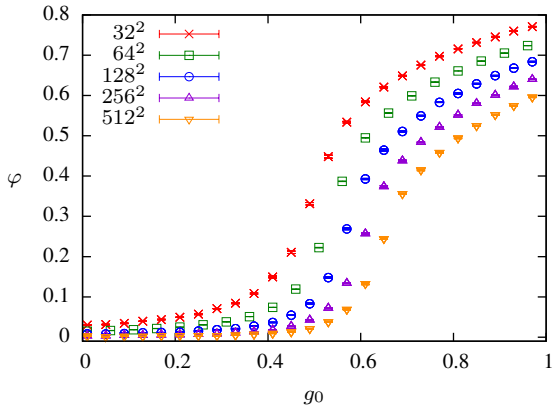

FIG. 3. The average field expectation value is shown as a function of g_0 for different lattice sizes and $N = 3$ for $S = g_0 N S_0$.

larger values of the coupling and we conclude that in the infinite volume limit the theory is in the symmetric regime for every finite value of the coupling, as predicted by the Mermin-Wagner theorem. It is also evident that finite volume effects are more important for large coupling. In particular, the observed behaviour might mimic an additional non-trivial fixed point of the RG flow. In Fig. 4 we show the β-function for the coupling g_0 in the simplest truncation using only the operator S_0. We observe that while the β-function is independent of the lattice volume, it depends on the parameter c_0 of the RG transformation. For $c_0 = 1$ the β function has an IR fixed point at vanishing coupling and stays positive even for large coupling. Tuning c_0 to larger values, the β-function develops a further zero crossing at finite coupling. However, this additional zero of the β-function is an artifact of the truncation. In Fig. 5 we show the ratio of correlation lengths of the original ensemble on the 64^2 lattice compared to the truncated ensemble on the 32^2 lattice. Truncation errors are assumed to be minimal for $\xi_{64}/\xi_{32} = 2$. For $c_0 = 1$ and $c_0 = 4$ significant deviations are visible. We find that $c_0 = 2.8$ provides a good matching for a large range of couplings. The corresponding beta function in Fig. 4 does not show an additional zero crossing, which coincides with earlier results [16]. For large g_0 the

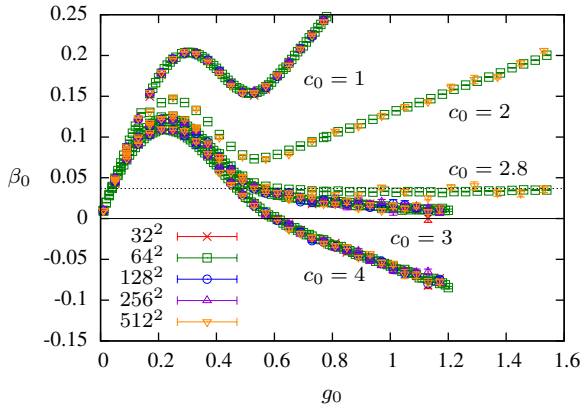

FIG. 4. The beta function β_0 for the simplest possible truncation and $N = 3$ is almost independent of the lattice volume. For $c_0 < 2.8$ it possesses only one fixed point at vanishing coupling. For $c_0 = 2.8$ it becomes constant for $g \to \infty$. The dotted line represents the analytical result for $N \to \infty$ and $g \to \infty$. For $c_0 > 2.8$ we find an additional fixed point at finite coupling which is an artifact of the truncation.

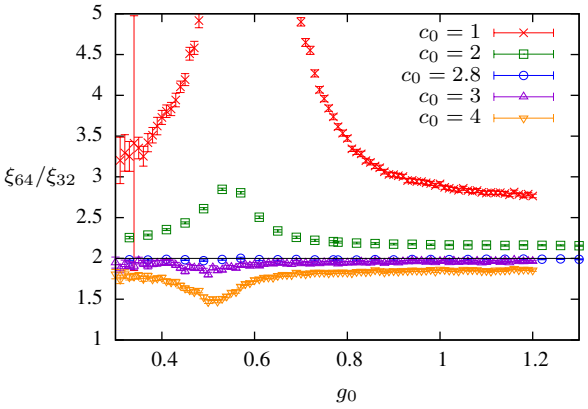

FIG. 5. The ratio of the correlation length for a 64^2 and 32^2 lattice is shown for different parameters of the RG transformation.

β function approaches a constant value corresponding to the large N result $\beta(N \to \infty, g \to \infty) = \ln(2)/(6\pi)$ [34]. In order to further improve on our truncation, we add a second operator S_1 and the resulting flow diagram for fixed $c_0 = 3$ and different lattice sizes is shown in Fig. 6. The flow is no longer independent of the volume and for the smallest lattice, which is 16^2, an additional fixed point in the (g_0, g_1)-plane emerges. However, going to larger lattice volumes, this fixed point shifts away towards larger couplings and thus we assume that in the continuum limit no additional fixed point of the RG flow exists.

The renormalized trajectory is the single trajectory that connects the Gaußian fixed point at the origin with the trivial fixed point at infinite coupling. The arrows plotted in Fig. 6 point towards the IR and therefore the fixed point at the origin is an IR fixed point while the fixed point at infinite coupling is UV attractive. Again we find that the structure of the flow diagram using the two-operator truncation matches the prediction from asymptotic freedom. The known results are very well repro-

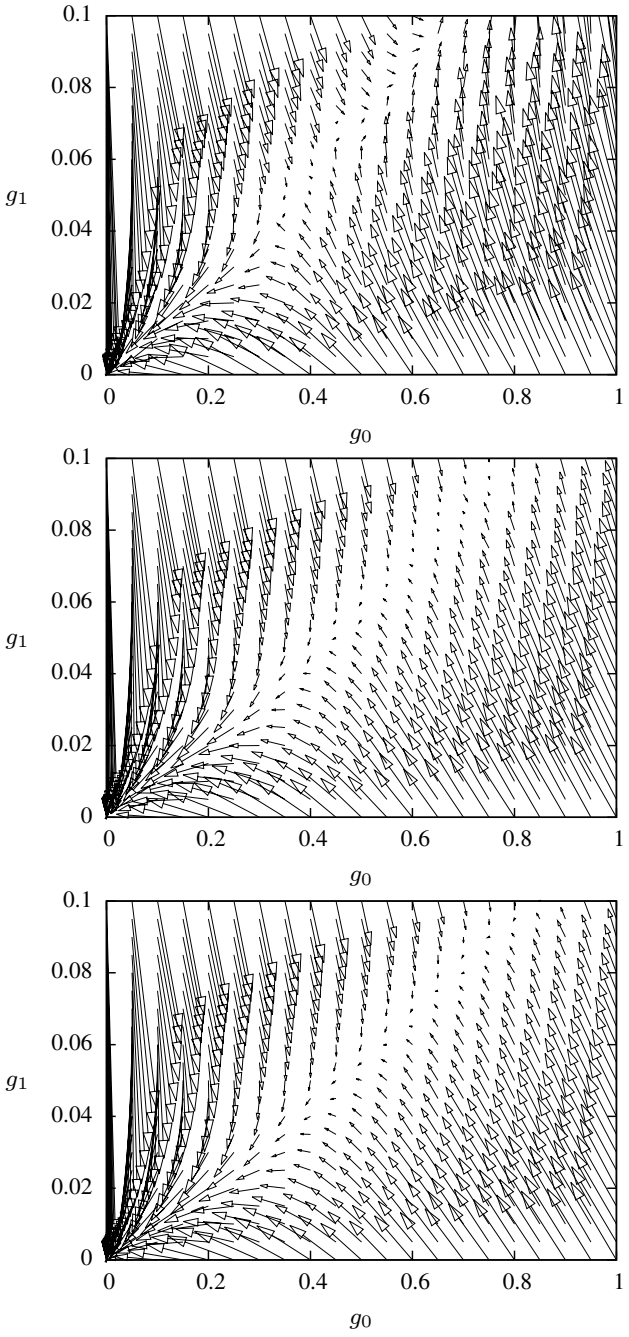

FIG. 6. Shown is the flow diagram for $c_0 = 3$ and $N = 3$ in the two operator truncation on a 16^2 (upper panel), 32^2 (middle panel) and 64^2 lattice (lower panel).

duced with our method and we proceed with the O(N) models in three spacetime dimensions.

V. FIXED POINTS OF THE RG FLOW IN THREE DIMENSIONS

As in two dimensions we first investigate the O(3) model. In Fig. 7 the order parameter φ for the spontaneous breaking of the O(N) symmetry is shown. The critical coupling in the

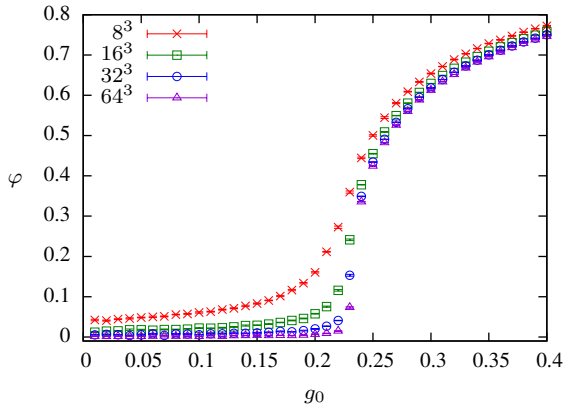

FIG. 7. The average field expectation value is shown as a function of g_0 for different lattice volumes.

thermodynamic limit is given by $g_0^c = 0.6862385(20)/3 = 0.2287462(7)$ [30]. On a 32^3 lattice, lattice artifacts are already sufficiently small for our purpose. Therefore most RG transformations considered in the present work are based on a transformation for a fine lattice with 32^3 points to a coarse lattice with 16^3 points. The critical coupling on the 32^3 lattice is $g_0^c = 0.22975(25)$.

A. One-parameter effective action

We begin with the simplest truncation possible by using the one-parameter action $S = g_0 N S_0$. We denote this scheme as $1 \to 1$ truncation, indicating the use of the one-parameter action in both ensemble creation and effective action ansatz.
As in two dimensions, the β function for this truncation is almost independent of the lattice size. Using different sizes, we see that our results from 8^3 and 16^3 already agree within their statistical error bars and therefore we are confident that our simulations on a lattice with 32^3 points do not suffer from large finite size effects.
In order to determine the optimization constant in the block-spin transformation, we again consider the correlation length of the two-point function. A perturbative calculation [10] yields $c_0^{\text{pert}} = 2.3$ for arbitrary N and a large number of subsequent RG steps. But computing the ratio of correlation lengths (see Figure 8), we see that there exists an optimal choice $c_0^{\text{opt}} = 3.35$ which leads to the desired value of $\xi_{16}/\xi_{32} = 2$. This value deviates significantly from $c_0^{\text{pert}} = 2.3$, indicating that the non-trivial fixed point is indeed a non-perturbative feature of the theory. Already with this simple setup, we find that the dimensionless β function, depicted in Fig. 9, exhibits the qualitative features that were expected from other methods [22–26]. In contrast to the two dimensional case, the β function shows a non-trivial fixed point g_0^* with $\beta(g_0^*) = 0$ for every value of c_0. This clearly points to the non-perturbative renormalizability of the O(3) -model and is directly related to a second-order phase transition. For the optimal choice c_0^{opt} we obtain $g_0^* = 0.2310(5)$. Systems with bare coupling $g_0 < g_0^*$

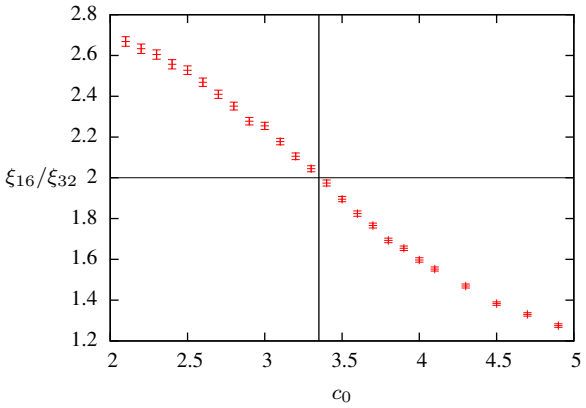

FIG. 8. The ratio of correlation lengths obtained by blocking a 32^3 lattice down to 16^3 using different optimization constants c_0. A value of $\xi_{16}/\xi_{32} = 2$ is expected to minimize truncation errors and we read off the optimal value $c_0^{\rm opt} = 3.35$ for $N = 3$.

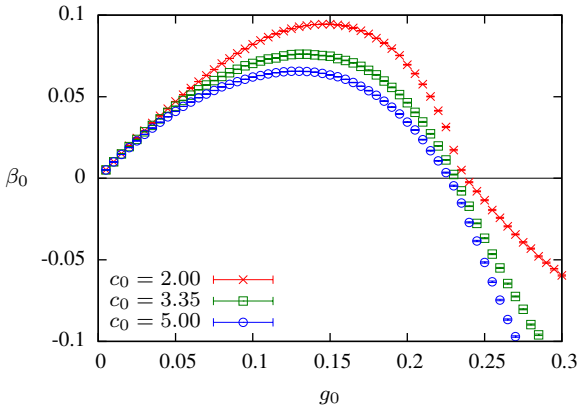

FIG. 9. The β function for the $1 \to 1$ truncation in three dimensions and $N = 3$ is shown for different values of c_0.

flow to the disordered phase in the IR which is controlled by the Gaußian fixed point at $g_0 = 0$, while systems with bare coupling $g_0 > g_0^*$ flow to the completely ordered phase described by $g_0 = \infty$ or $1/g_0 = 0$. These two fixed points correspond to the expected low-temperature fixed point at infinite coupling (absolute order) and the expected high-temperature fixed point at zero coupling (absolute disorder). The critical hypersurface is reduced to a single point g_0^* in this truncation and the operator S_0 corresponds to a *relevant* direction of the RG flow.

Using the information provided by thermodynamical observables like e.g. the susceptibility of the order parameter, we can determine the *critical point* g_0^c where the correlation length of the system diverges at infinite volume. In general theory space, it is the point of intersection between the critical hypersurface and the line where $g_i = 0$ except g_0. A lattice simulation starting at g_0^c in the UV will flow along the critical line into the non-trivial fixed point and observables measured on this ensemble reflect the macroscopic physics at this point. Please note that g_0^c need not be identical to g_0^* due to truncation errors that affect the value for g_0^*. Of course, without truncation errors the fixed point is located at the critical surface. We now proceed to discuss higher-order truncations which take additional operators into account and provide a more complete picture of the flow of the effective action.

B. Higher-order truncations

In the preceding sections we have seen that near the non-trivial fixed point the operator S_0 defines a relevant direction. In this section we include more operators in the effective action in order to find the total number of relevant directions. Figure 10 (upper panel) shows the global flow diagram for the truncation using two operators $S = g_0 NS_0 + g_1 NS_1$, both for ensemble generation as well as in the demon method ($2 \to 2$ truncation). The blockspin transformation is optimized in

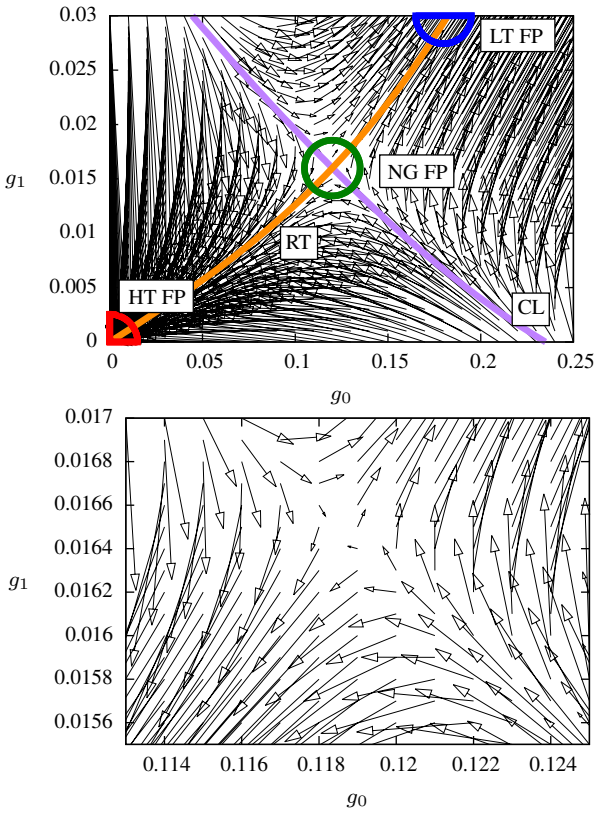

FIG. 10. The flow diagram using the $2 \to 2$ truncation in three dimensions and $N = 3$ clearly shows a non-Gaußian fixed point (NG FP) in the center of the plot in the upper panel. The critical line (CL) and renormalized trajectory (RT) intersect at the NG FP. The lower panel shows the vicinity of the NG FP. The RG parameters for this flow diagram are $c_0 = 3.1$ and $c_1 = 2.5$.

the same way as for the action with a single parameter. Our choice for the parameters is $c_0 = 3.1$ and $c_1 = 2.5$ and it leads to a correlation length ratio of around 2 in the vicinity of the fixed point. Note that this choice for the parameters is not unique if we only tune the correlation length to the desired value. In general we have to consider higher correlation functions as well. Below we will also discuss other choices

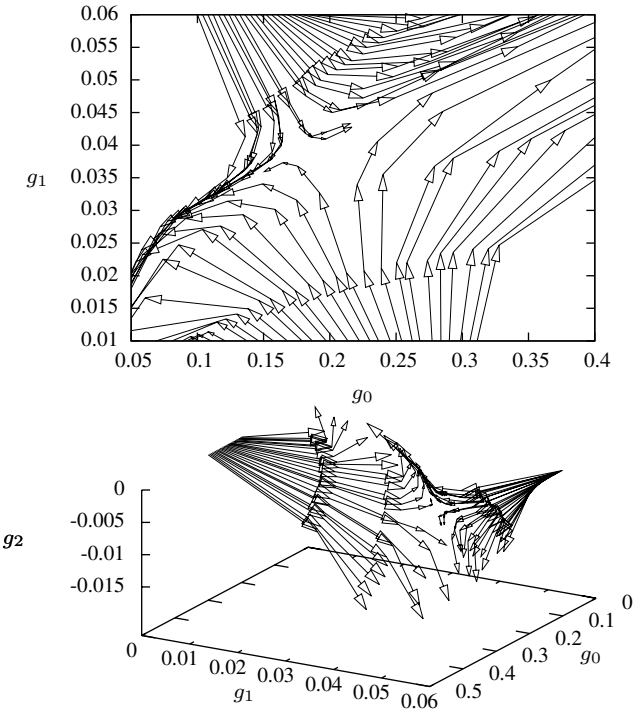

FIG. 11. Using a shooting technique, the RG trajectories for the $3 \to 3$ truncation with operators S_0, S_1 and S_2 reveal an analogous structure to the $2 \to 2$ case. The projection on the g_0-g_1 axis in the upper panel shows only a single relevant direction at the non-Gaußian fixed point. The lower panel shows that the trajectories first approach the fixed point regime and afterwards flow along the renormalized trajectory to the respective IR fixed points.

for the parameters and its influence on quantitative features of the flow diagram as for example the position of the fixed point or critical exponents. Nevertheless as in the one parameter case the choice of the parameters does not change the qualitative flow diagram. Again, we detect a high temperature fixed point (HT FP) at zero coupling in the lower left corner as well as a low temperature fixed point (LT FP) at infinite coupling. Also a non-trivial fixed point (NG FP) in the center of the flow diagram is clearly visible. The values of the couplings at the fixed point, $g_0 = 0.119(1)$, $g_1 = 0.0164(2)$, can be determined from Fig. 10 (lower panel). As expected, the 'velocity' along a trajectory gets small in the fixed point regime. Furthermore, we find that the position of the fixed point in this two parameter truncation is almost independent of the lattice volume. But, in contrast to the one-parameter truncation, it depends strongly on the constant c_0 and to a lesser degree on the remaining constants. A change of c_0 results in a displacement of the fixed point along the critical line.

The flow diagram is split by a separatrix which defines the critical line (CL) extending from the lower right to the upper left corner. Trajectories that lie above this line will flow into the low temperature fixed point while trajectories below this line flow into the high temperature fixed point. This indicates a relevant direction analogous to the simple one-parameter truncation of the preceding section. The second direction though is an irrelevant one and the corresponding eigenvalue of the stability matrix is negative. The single trajectory that is identical with the critical line will flow into the non-trivial fixed point, either from below or above. The critical line is the intersection of the critical hypersurface in general theory space with the g_0-g_1 plane that constitutes our truncation. From the traditional lattice perspective, the critical line corresponds to a fine-tuned set of bare couplings (g_0, g_1) at different UV cutoffs. Starting a simulation on the critical line results in a measurement of the critical physics at the non-trivial fixed point and is generically used to take the continuum limit, since the lattice spacing in units of the correlation length becomes small as the critical point is approached.

There exists another interesting line which connects all three fixed points and acts as an attractor for the RG trajectories. It is called the renormalized trajectory (RT) and singles out a unique trajectory that defines a theory that is both IR and UV complete, starting at the non-trivial fixed point in the UV and flowing into the high temperature or low temperature fixed point in the IR. As expected, the RT does not attract the trajectories in the vicinity of the high temperature fixed point, where the fixed point behaviour dominates [1].

Starting on the g_0 axis, which corresponds to the usual lattice action of the Heisenberg ferromagnet, and integrating out all fluctuations, one can only reach either one of the trivial fixed points or the non-trivial fixed point. In this sense, it is legitimate to consider them as *infrared fixed points*. From universality arguments one expects that the non-Gaußian fixed point corresponds to the well-known Wilson-Fisher fixed point of the linear sigma model. We find that a similar structure to our results emerges in this model [35].

But the Heisenberg ferromagnet is an effective theory that is well defined only for a finite UV cutoff, in contrast to *asymptotically safe theories* that are defined on all scales. Fundamental field theories correspond to theories on the renormalized trajectory and the direction of the renormalization group flow shows that the non-trivial fixed point governs the ultraviolet physics of these theories. Thus, this non-trivial fixed point acts as an *ultraviolet fixed point* of the RG flow.

For the asymptotic safety scenario to hold, the number of relevant directions at the non-Gaußian fixed point must be finite. Hence we proceed to determine the flow diagram for the $3 \to 3$ and $4 \to 4$ truncation, which include the operators $\{S_0, S_1, S_2\}$, $\{S_0, S_1, S_3\}$ and $\{S_0, S_1, S_2, S_3\}$ respectively. An overview over the full flow diagram for the operators $\{S_0, S_1, S_2\}$ is presented in Figure 11 and it is evident that only irrelevant directions are added to the truncation. The global structure of the flow diagram is similar to the $2 \to 2$ truncation and shows two trivial IR fixed points and one non-trivial UV fixed point. Figure 12 (upper panel) shows a detailed view of the the fixed point regime. The fixed point is located at $(g_0, g_1, g_2) = (0.13(1), 0.016(1), -0.0015(5))$. In the center panel of Figure 12 the $3 \to 3$ trunca-

[1] For this reason the matching method is not applicable in the vicinity of the high temperature fixed point since it relies on the assumption that the trajectories approach the renormalized trajectory within a few RG steps [34].

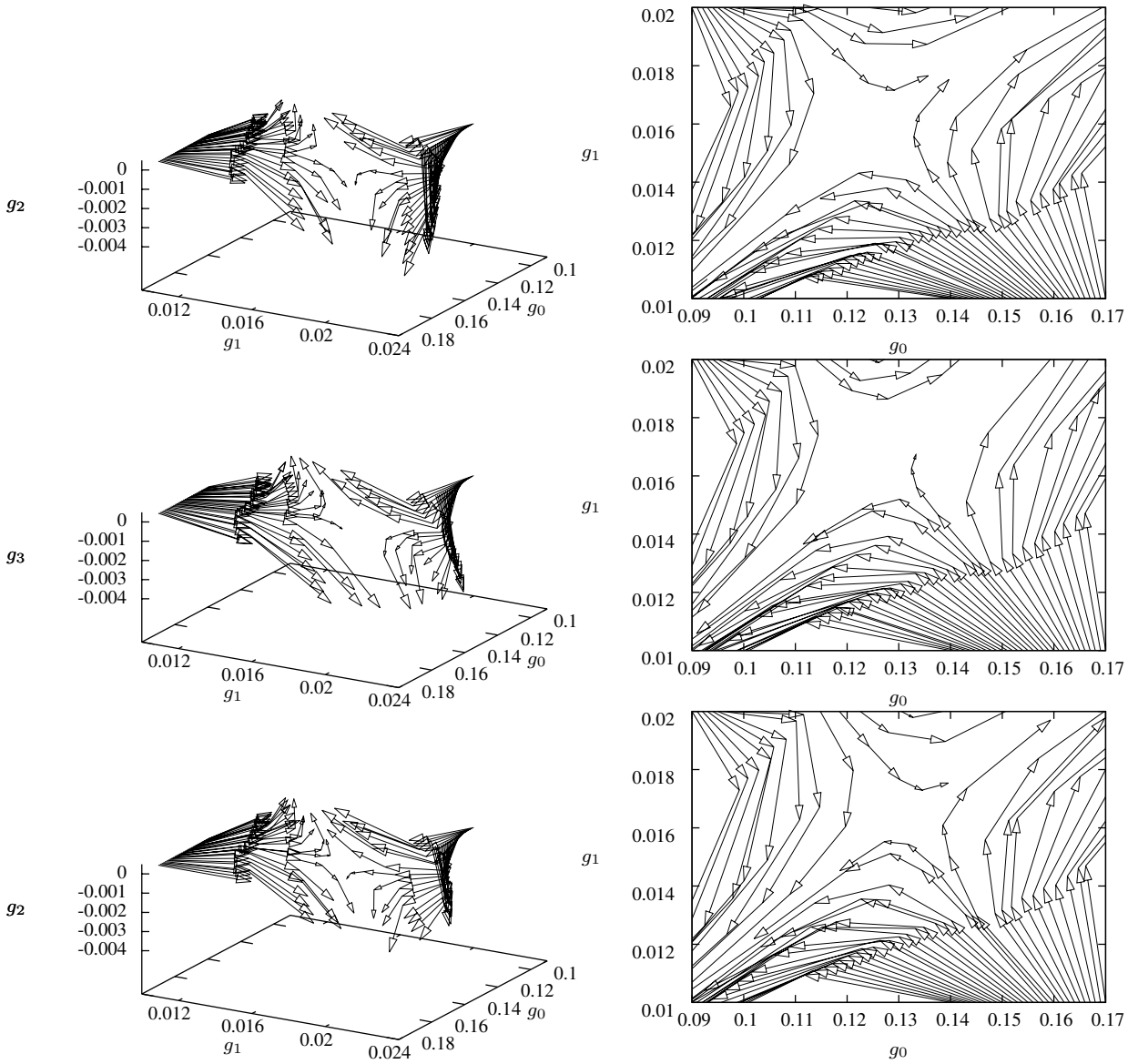

FIG. 12. For higher order truncations with operators $\{S_0, S_1, S_2\}$ in the upper panel, $\{S_0, S_1, S_3\}$ in the center panel and $\{S_0, S_1, S_2, S_3\}$ in the lower panel the fixed point structure of the resulting flow diagram remains the same as for the $1 \to 1$ and $2 \to 2$ truncation.

tion with operators $\{S_0, S_1, S_3\}$ is presented. The resulting flow diagram is again very similar and we find that even the position of the fixed point at $(g_0, g_1, g_3) = (0.13(1), 0.016(1), -0.0015(5))$ matches the prior result within the resolution of the flow diagram. Finally Fig. 12 (lower panel) shows the results for the $4 \to 4$ truncation. Again the fixed point structure remains unchanged. In this truncation the position of the fixed point is at $(g_0, g_1, g_2, g_3) = (0.13(1), 0.016(1), -0.0015(5), -0.0015(5))$. In conclusion, we observed that the fixed point structure does not change if we add further operators. We always find just one relevant direction at the non-Gaußian fixed point. In addition the position of the fixed point is stable against including the higher derivative operators S_2 and S_3. This clearly points to the existence of a non-Gaußian fixed point of the RG transformation and thus we are led to believe that the asymptotic safety scenario applies to the O(3) nonlinear sigma model in three dimensions.

C. Critical exponents

Following the universality hypothesis, it is generally assumed that the linear and nonlinear O(N) models are in the same universality class, since they have the same range of interaction and symmetries. This assumption is supported by several computations based on very different approximations, cf. for instance [29, 36, 37] or the overviews [38, 39].
Furthermore, critical exponents are universal, in contrast to the position of the fixed point, and this allows us to compare

our results to the functional RG studies of the nonlinear O(N) models in [27]. Here we restrict ourselves to the scaling properties of the correlation length, described by the exponent ν, since it is directly related to the relevant eigenvalue $-\theta_r$ of the stability matrix by $\nu = \theta_r^{-1}$.

Using the simple $1 \to 1$ truncation, the inverse of the thermodynamic critical exponent ν corresponds to the negative slope of the lattice beta function in the vicinity of a fixed point, depicted in Fig. 9. As expected, we find the trivial values $\nu \approx -1$ and $\nu \approx 1$ for the high-temperature and low-temperature fixed points, respectively. These values are almost independent of c_0. For the non-trivial fixed point, on the other hand, the value depends on the choice for c_0, and this is shown in Fig. 13. For the optimal constant $c_0 = 3.35$

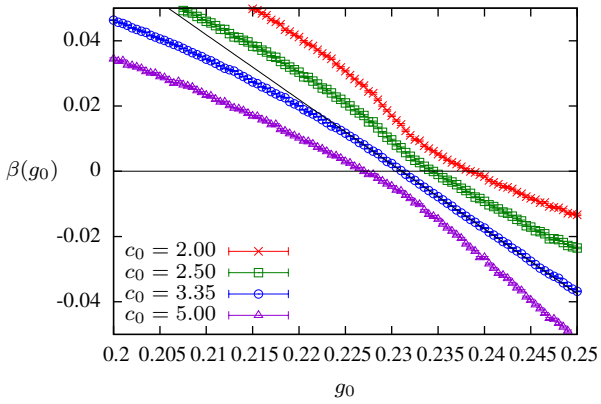

FIG. 13. β function in the vicinity of the fixed point in the $1 \to 1$ truncation for the O(3) -model and various values of c_0.

we read off the critical exponent $\nu(1 \to 1) = 0.51(1)$ for $N = 3$, which is to be compared with the value $0.7112(5)$ in [30] obtained from a dedicated Monte Carlo simulation combined with high-temperature expansions. In Fig. 14 the critical exponent is shown as a function of c_0. Again one sees

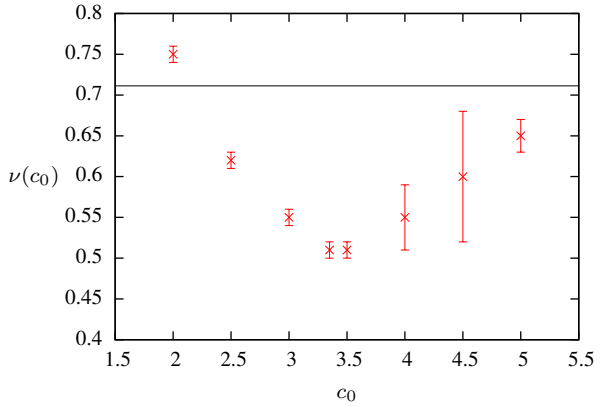

FIG. 14. The critical exponent ν is shown as a function of c_0.

that a careful optimization of the blockspin transformation is important in order to extract accurate results for the critical exponents.

The next improvement is to allow 2 operators in the effective action, denoted as $1 \to 2$ truncation. The critical exponent is determined as the negative slope of the projected β-function on the g_0 axis at the position of the fixed point for the $1 \to 1$ truncation. For the optimized $c_0 = c_0^{\text{opt}}$ we obtain $\nu(1 \to 2) = 0.55(2)$. This is already significantly closer to the expected value compared with the simple $1 \to 1$ truncation.

We can further improve our estimate by moving on to the $2 \to 2$ truncation. Depicted in Figure 15 (upper panel) is the eigenvalue θ_r of the matrix (18), which at a critical point becomes the stability matrix, and again it takes the trivial values at the high temperature or low temperature fixed point. While the plot shows strong variations of the eigenvalue at the

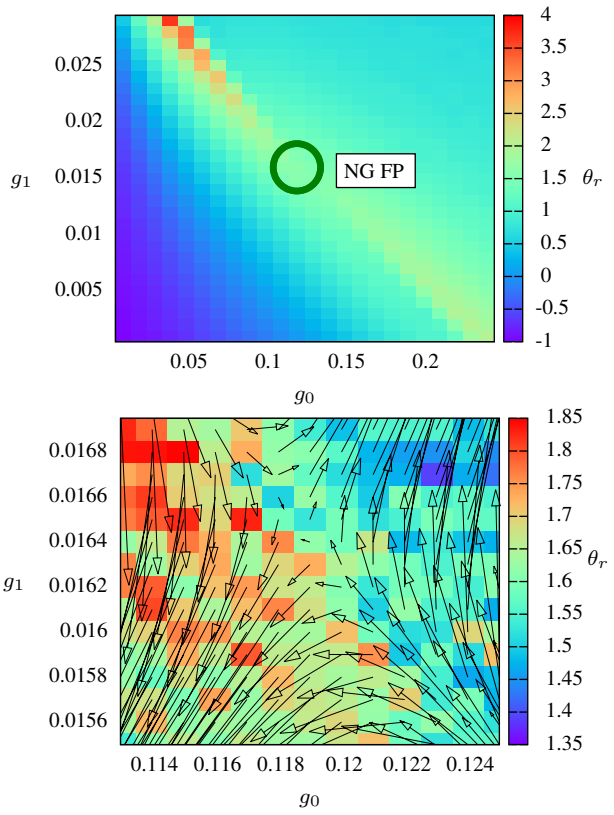

FIG. 15. The critical exponent ν is related to the eigenvalue θ_r of the stability matrix corresponding to the relevant direction. The RG parameters for this flow diagram are $c_0 = 3.1$ and $c_1 = 2.5$.

upper left and lower right corner of the parameter space, it becomes smooth in the vicinity of the non-trivial fixed point, see Fig. 15 (lower panel). From an average over the fixed point region we obtain the value of $\nu(2 \to 2) = 0.62(3)$, which already deviates less than 15% from the literature value. We stress that in the present work we are mainly concerned with the flow diagram and fixed point structure of non-linear O(N) -models such that our method is not to be seen as a replacement of dedicated high-precision Monte Carlo determination of critical exponents. It is however possible to estimate these quantities in addition to the flow diagram with a reasonable precision.

In the $2 \to 2$ truncation we can also extract the critical ex-

ponent corresponding to the irrelevant direction of the flow, see Fig. 16. It takes the trivial value $\theta_{ir} = -1$ at the high

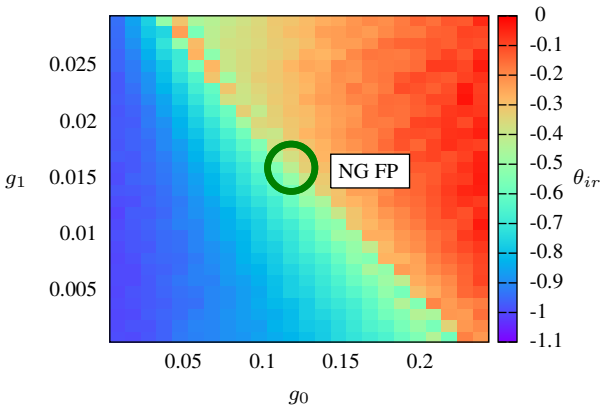

FIG. 16. The critical exponent corresponding to the irrelevant direction is negative at the high temperature and non-Gaußian fixed point. The RG parameters for this flow diagram are $c_0 = 3.1$ and $c_1 = 2.5$.

temperature fixed point and $\theta_{ir} \approx -0.44$ at the non-Gaußian fixed point. In order to check for the stability of our method we calculated the critical exponent also for the RG parameters $c_0 = 3.4$ and $c_1 = 1.0$. We obtained the value $\nu = 0.65(3)$. Within statistical errors this agrees with the value for ν obtained before.

For the $3 \to 3$ truncation we set the RG parameter belonging to the additional operator to zero, i.e. $c_0 = 3.1$, $c_1 = 2.5$ and $c_2 = 0$. In this truncation we obtain three critical exponents:

$$\begin{aligned} \theta_r &= 1.57(5)\,, \\ \theta_{ir}^1 &= -0.52 + 0.05\mathrm{i}\,, \\ \theta_{ir}^2 &= -0.86 - 0.05\mathrm{i}. \end{aligned} \tag{33}$$

The exponent of the correlation length is then $\nu(3 \to 3) = 0.64(3)$. Within statistical errors this is almost no improvement compared to the $2 \to 2$ truncation.

Our analysis of the critical exponents indicates that the high temperature fixed point has only irrelevant directions, i.e. all critical exponents are negative. The exponents corresponding to the operators S_0 and S_1 take the value $\theta_{0,1} = -1$. The non-Gaußian UV fixed point has one positive critical exponent, while the other critical exponents are negative. This again verifies the asymptotic safety scenario for the nonlinear sigma model in three dimensions. Table I summarizes our results for the critical exponents. For comparison we also show results obtained with Monte Carlo simulations (MC), high temperature expansion (HT), RG expansion (RG) and functional RG (FRG). With increasing truncation order our results approach the very precise values obtained with other methods, indicating that our derivative expansion converges to the correct results. For even higher truncations the computation of critical exponents becomes very time consuming and the statistical errors become larger than the deviation from the values in the literature. Furthermore the optimization of the blockspin transformation becomes increasingly difficult. Nevertheless results are good enough to show that the non-Gaußian UV fixed point

Method	ν	ν/ν_{MC}
$1 \to 1$ trunc. ($c_0 = 3.35$)	0.51(1)	~ 0.71
$1 \to 2$ trunc. ($c_0 = 3.35$)	0.55(2)	~ 0.77
$2 \to 2$ trunc. ($c_0 = 3.1,\ c_1 = 2.5$)	0.62(3)	~ 0.87
$2 \to 2$ trunc. ($c_0 = 3.4,\ c_1 = 1.0$)	0.66(4)	~ 0.93
$3 \to 3$ trunc. ($c_0 = 3.1,\ c_1 = 2.5,\ c_2 = 0$)	0.64(3)	~ 0.90
FRG [27]	0.704	~ 0.99
MC [30]	0.7112(5)	1
RG [31]	0.706	~ 0.99
HT [29]	0.715(3)	~ 1

TABLE I. Results for the critical exponent ν for different truncations and $N = 3$ compared to the very precise results of the Monte Carlo estimate MC.

indeed belongs to a well-known class of second order phase transitions.

VI. THE LARGE N LIMIT

For large values of N we can compare our results with those from the analytical large N and RG expansions in [40] and [31], respectively. In Fig. 17 the β-function in the $1 \to 1$ truncation is shown for different N at the optimized value for $c_0(N)$. For every value of N a non-trivial fixed point exists,

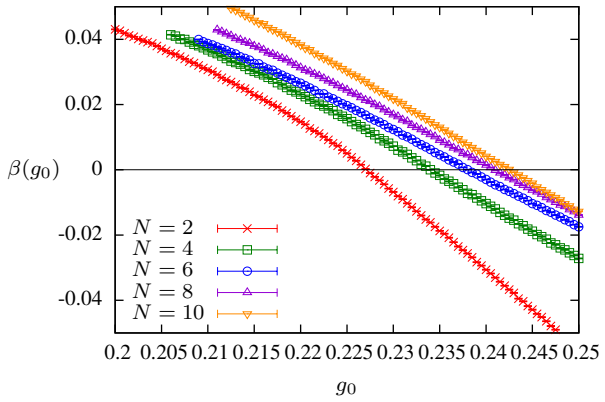

FIG. 17. Shown is the β function in the one parameter truncation for various N and optimized blockspin transformation.

but the slope at the fixed point changes. In order to connect to the large N limit, we repeat the computation of the critical exponent ν in the simple $1 \to 1$ truncation for N up to 10. The results are shown in Fig. 18. Starting from $N = 2$, where the estimate deviates from the comparative RG data by $\nu/\nu_{RG} \approx 40\%$, we see a significant improvement for intermediate $N < 8$. However, going to even larger N, the behaviour changes and our results significantly underestimate the correct values. It is evident that we do not reproduce the analytically known result of $\nu = 1$ for $N \to \infty$. This change of behaviour is not only visible in the critical exponents but also shows up in the value of the optimization constant c_0. From the perturbative analysis [10], we know that for large N the RG param-

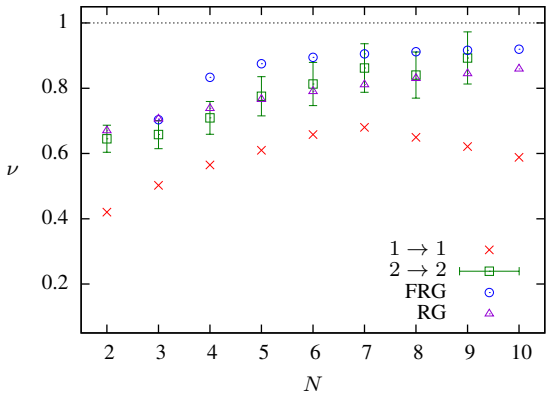

FIG. 18. The critical exponent ν is shown for the $1 \to 1$ and $2 \to 2$ truncation depending on N. We compare our data to results using the Functional RG [27] and RG expansion [31]. In the large N limit we expect $\nu = 1$.

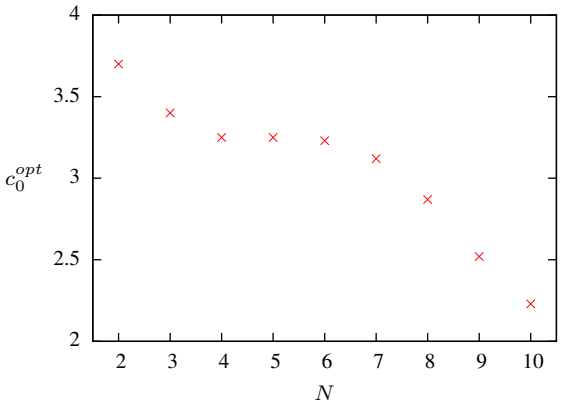

FIG. 19. The optimization constant c_0 in the $1 \to 1$ truncation is shown for various N.

eter is proportional to $\frac{N}{N-1}$, i.e. we expect $c_0(N)$ to become constant for large N. Indeed in Figure 19 we see a plateau for intermediate values of N. Unfortunately, for $N \gtrsim 7$ the optimization constant decreases rapidly. We interpret this unexpected behaviour as a breakdown of our simple one parameter truncation for large N. If the effective action does not capture the relevant physics anymore, then we should not expect to find reliable values for the critical exponents. Although we can tune the ratio of two-point functions to the desired value, higher correlation functions should indicate that, within our truncation, the IR physics changes under the RG transformation.

We might try to improve the situation by including higher order operators. For the $2 \to 2$ truncation we calculated the critical exponents up to $N = 9$ and actually see a significant improvement over the $1 \to 1$ truncation, see Fig. 18. It turns out that, compared to the literature, we get the best results if we set the RG parameter c_0 to the values obtained in the simplest truncation for $N \leq 6$ and to the plateau value for $N > 6$. For the second operator we choose $c_1 = 1.0$. We checked that the ratio of the correlation length is approximately 2 in the vicinity of the fixed point for this set of parameters. In Figure 20, we show that for different N the general structure of the flow diagram persists. Only the non-universal location of the non-Gaußian fixed point varies.

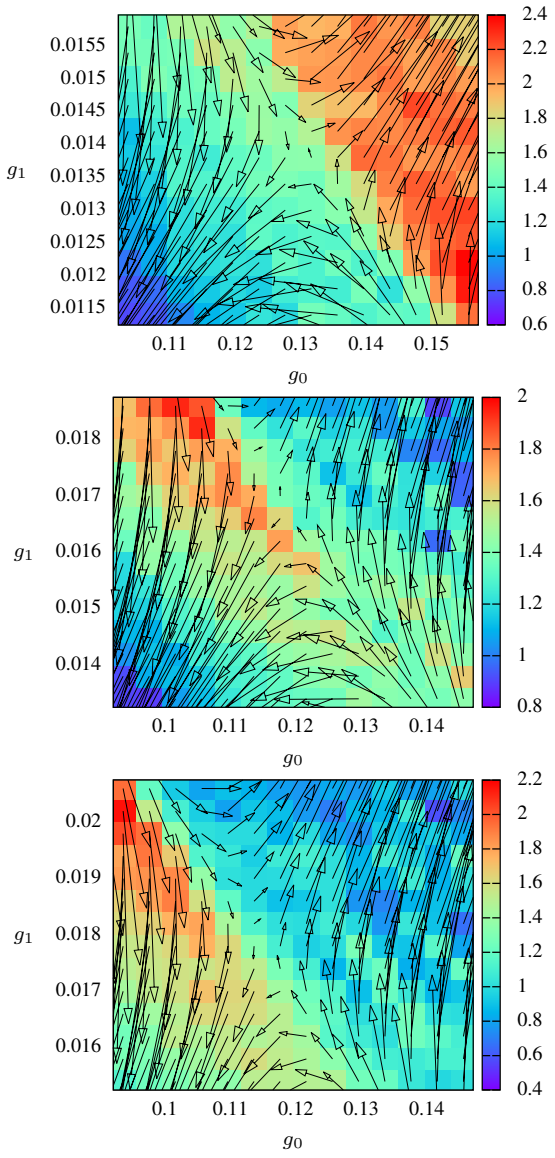

FIG. 20. Flow diagram using the $2 \to 2$ truncation in three dimensions for O(2), O(4) and O(6)-models. The global structure is the same as for the O(3) -model. The background color encodes the eigenvalue θ_r of the matrix in (18), which near a critical point is related to the critical exponent of the correlation length.

Unfortunately the fine-tuning of the RG parameter and the computation of critical exponents becomes increasingly difficult for even larger N. We again observe that for $N > 9$ our truncation breaks down and additional operators are needed to obtain reliable results for the critical exponents. Nevertheless the fixed point structure itself remains stable. Our final results are compiled in Table II and Figure 18.

N	2	3	4	5	6	7	8	9	10
$1 \to 1$ truncation	0.42	0.51	0.57	0.63	0.65	0.68	0.65	0.62	0.58
$2 \to 2$ truncation	0.64(4)	0.66(4)	0.71(5)	0.78(6)	0.81(6)	0.86(7)	0.84(7)	0.89(8)	-
FRG [27]	-	0.704	0.833	-	0.895	-	0.912	-	0.920
HT exp. [29]	0.677(3)	0.715(3)	0.750(3)	-	0.804(3)	-	0.840(3)	-	0.867(4)
RG exp. [31]	0.607	0.706	0.738	0.766	0.790	0.811	0.830	0.845	0.859

TABLE II. Results for the critical exponent ν for different N obtained using different methods.

VII. CONCLUSIONS

We have discussed and applied a method that allows to compute the global flow diagram of a model from numerical simulations. In contrast to the MCRG matching technique, our method does not need exponentially large lattices and works even in the vicinity of a Gaußian fixed point, where the renormalized trajectory no longer acts as an attractor for the RG flow. Furthermore, we have shown that systematic uncertainties from a truncation of the effective action can be mitigated efficiently by an optimization of the RG transformation.

The nonlinear sigma model is asymptotically free in two dimensions and we have reproduced the expected structure of the flow diagram, showing two trivial fixed points corresponding to the behaviour at very low and very high temperature, already using the simplest possible truncation that only includes a nearest-neighbor interaction. Using a two-operator truncation, we have clarified the role of the finite volume behaviour on the flow diagram and argued that an additional non-trivial fixed point is a lattice artifact.

It has long been known that the three-dimensional O(3) -model shows a second-order phase transition that separates a phase of broken O(N) symmetry and a symmetric phase. We have shown that this phase transition corresponds to an ultraviolet fixed point with *one* relevant direction by using a truncation that includes all (allowed by symmetry) operators up to fourth order in the momentum. It is possible to define a theory along the renormalized trajectory that is IR- and UV-complete. We conclude that the asymptotic safety scenario is fulfilled and the model is renormalizable in a non-perturbative setting.

While the general structure of the flow diagram does not depend on the specific RG scheme the critical exponents vary since the systematic error depends on the specific optimization constant. We find that our method is able to predict the critical exponents within a reasonable accuracy but can not compete to designated high precision MC-techniques that are free of truncation errors [30]. We find that our estimates for the critical exponents improve for larger truncations but fail to reproduce the exact $N \to \infty$ limit.

Using functional renormalization group techniques, the full flow diagram for the present model was obtained already in an earlier publication [27]. We find that the qualitative structure of the flow diagrams are the same. However, the MCRG method is more stable than the FRG method and leads to more robust results for different truncations. In particular, we do not find a sudden disappearance of the non-trivial fixed point for a certain truncation including the operator S_2 (28). Furthermore, we stress that lattice techniques provide the opportunity to obtain additional information beyond the chosen truncation by a direct measurement of the Green's functions. We have used this knowledge to determine the optimal constants in the improved RG transformation. In addition we compared the location of the critical point, determined by the susceptibility of the order parameter, to the location of the fixed point, determined by the zero crossing of the beta function and hence amendable to truncation errors. We find that these points do not coincide in general. For the simplest truncation we observe a small deviation even for the optimal value of the RG constant. For higher truncations, the fixed point location matches the critical surface within statistical errors. Another interesting observation is that the β function in the lowest truncation for two and three dimensions does not depend on the lattice size.

Our method can be generalized to other systems, especially including fermionic degrees of freedom, and thus allows to determine the more complex flow diagrams of e.g. the Thirring model [41]. The method might also be used to study lattice quantum gravity [42, 43] where it is difficult to define observables that capture the infrared physics of the theory. In contrast to the matching technique, the method used in the present work does not rely on the computation of correlation functions but only on an appropriate RG transformation that acts directly on the spacetime triangulations used.

ACKNOWLEDGMENTS

This work was supported by the DFG-Research Training Group "Quantum- and Gravitational Fields" GRK 1523 and DFG grant Wi777/11 and by the Helmholtz International Center for FAIR within the LOEWE initiative of the State of Hesse. We thank Raphael Flore for his active collaboration and Jens Braun, Axel Maas, Roberto Percacci, Martin Reuter, Omar Zanusso and Luca Zambelli for interesting discussions or useful comments. Simulations were performed on the Omega HPC cluster at the University of Jena and the LOEWE-CSC at the University of Frankfurt.

Appendix A: Two Alternative Formulations of a Fourth-Order Derivative Expansion

In this article we study the full fourth order derivative expansion of the theory, formulated in terms of explicitly constrained variables $\boldsymbol{\phi} \in \mathbb{R}^N$ with $\boldsymbol{\phi}\cdot\boldsymbol{\phi} = 1$. In order to compare the results with previous studies of the same system by means of the Functional Renormalization Group (FRG) [27], one has to know the relation between both parametrizations of the action functional. The FRG computations in [27] were performed for the covariant formulation

$$\begin{aligned}\Gamma[\varphi] =& \frac{1}{2}\int d^3x\, \zeta h_{ab}\partial_\mu\varphi^a\partial^\mu\varphi^b \\ &+ \alpha h_{ab}(\nabla_\mu\partial^\mu\varphi)^a(\nabla_\nu\partial_\nu\varphi)^b \\ &+ L_1(h_{ab}\partial_\mu\varphi^a\partial_\nu\varphi^b)^2 \\ &+ L_2(h_{ab}\partial_\mu\varphi^a\partial^\mu\varphi^b)^2\,,\end{aligned} \tag{A1}$$

in terms of unconstrained fields $\varphi \in \mathbb{R}^{N-1}$, where $(\nabla_\mu\partial^\mu\varphi)^a = \partial^2\varphi^a + \Gamma^a_{bc}\partial_\mu\varphi^b\partial^\mu\varphi^c$ and Γ^a_{bc} is the Christoffel symbol corresponding to the metric $h_{ab}(\varphi)$. In order to determine the relation between (A1) and (19), one can choose stereographic coordinates,

$$h_{ab} = \frac{\delta_{ab}}{(1+\varphi^2)^2} \quad \text{with } \varphi^2 = \sum_{a=1}^{N-1}\varphi^a\varphi^a\,, \tag{A2}$$

for an unconstrained parametrization of (A1) and apply an inverse stereographic projection,

$$\varphi^a = \frac{\phi^a}{1+\phi^N} \quad \text{for } i = 1,..,N-1\,, \tag{A3}$$

such that

$$\begin{aligned}\Gamma[\varphi(\phi)] =& \frac{1}{2}\frac{\zeta}{4}\,\partial_\mu\phi\partial^\mu\phi + \frac{1}{2}\frac{\alpha}{4}\,\partial^2\phi\partial^2\phi \\ &+ \frac{1}{2}\frac{L_1}{16}\,(\partial_\mu\phi\partial_\nu\phi)^2 \\ &+ \frac{1}{2}\frac{L_2-4\alpha}{16}\,(\partial_\mu\phi\partial^\mu\phi)^2\,.\end{aligned} \tag{A4}$$

A comparison with (19) yields

$$g_0 = \frac{\zeta}{4}\,,\quad g_1 = \frac{\alpha}{4}\,,\quad g_2 = \frac{L_1}{16}\,,\quad g_3 = \frac{L_2-4\alpha}{16}\,. \tag{A5}$$

Appendix B: The LHMC algorithm

In the case of nonlinear sigma models with only the standard interaction term S_0, cluster algorithms have proven to be the most efficient way to update the scalar field in Monte-Carlo simulations. In its original version, the cluster algorithm assumes that only nearest neighbor interactions are present and hence is not directly applicable in the presence of higher derivative operators. Thus we employ a local version of the hybrid Monte-Carlo algorithm (LHCM) where single site variables are evolved in an HMC algorithm. This ansatz relies on local interactions and is applicable theories without dynamical fermions. The formulation is given entirely in terms of SO(N) -Lie-group and Lie-algebra elements, see also [44]. To update the normalized scalar field we set

$$\Phi_x = \mathcal{O}_x\Phi_0 \quad \text{with} \quad \mathcal{O}_x \in \text{SO(N)} \tag{B1}$$

and constant Φ_0. The change of variables $\Phi_x \to \mathcal{O}_x$ converts the induced measure on $S^{N-1} \subset R^N$ into the Haar measure of SO(N) . Without interaction the rotation matrices $\mathcal{O}_x$ will evolve freely on the group manifold SO(N) . The *free evolution* on a semisimple group is the Riemannian geodesic motion with respect to the Cartan-Killing metric

$$ds^2 \propto \operatorname{tr}\left(d\mathcal{O}\mathcal{O}^{-1}\otimes d\mathcal{O}\mathcal{O}^{-1}\right). \tag{B2}$$

The LHMC dynamics may be naturally derived from a Lagrangian of the form

$$L = -\frac{1}{2}\sum_x \operatorname{tr}\left(\dot{\mathcal{O}}_x\mathcal{O}_x^{-1}\right)^2 - S[\,\mathcal{O}], \tag{B3}$$

where 'dot' denotes the derivative with respect to the fictitious time parameter τ. The Lie-algebra valued pseudo-momenta conjugated to the site variable $\mathcal{O}_x$ are given by

$$\mathfrak{P}_x = \frac{\partial L}{\partial\left(\dot{\mathcal{O}}_x\mathcal{O}_x^{-1}\right)} = -\dot{\mathcal{O}}_x\mathcal{O}_x^{-1}. \tag{B4}$$

The Legendre transform yields the following pseudo-Hamiltonian

$$H = -\frac{1}{2}\sum_x \operatorname{tr}\mathfrak{P}_x^2 + S[\,\mathcal{O}]. \tag{B5}$$

Note that for $\mathcal{O}_x \in$ SO(N) the momenta are antisymmetric such that the kinetic term is positive. The equations of motion for the momenta are obtained by varying the Hamiltonian,

$$\delta H = -\sum_x \operatorname{tr}\mathfrak{P}_x\{\dot{\mathfrak{P}}_x - F_x\} \quad \text{and} \quad F_x = \delta S[\,\mathcal{O}]. \tag{B6}$$

In the simplest case of only nearest neighbor interactions the *force* is given by

$$F_x = g_0\,\Phi_x\Big(\sum_{x,\mu}\Phi_{x+\mu}\Big)^{\mathsf{T}}. \tag{B7}$$

The variational principle implies that the projection of the terms between curly brackets onto the Lie-algebra $\mathfrak{so}(N)$ vanishes,

$$\dot{\mathfrak{P}}_x = F_x\big|_{\mathfrak{so}(N)}. \tag{B8}$$

There is a freedom of choice of F and we determine it by a projection on a trace-orthonormal basis $\{T_a\}$ of $\mathfrak{so}(N)$. Then the LHMC equations read

$$\dot{\mathcal{O}}_x = -\mathfrak{P}_x\mathcal{O}_x \quad \text{and} \quad \dot{\mathfrak{P}}_x = \sum_b \operatorname{tr}\left(F_xT_b\right)T_b\,. \tag{B9}$$

To solve these equations of motion numerically, we employ a time reversible leap frog integrator which uses the integration scheme

$$\begin{aligned}\mathfrak{P}_x(\tau+\tfrac{1}{2}\delta\tau) &= \mathfrak{P}_x(\tau) + \tfrac{1}{2}\delta\tau\,\dot{\mathfrak{P}}_x(\tau)\\ \mathcal{O}_x(\tau+\delta\tau) &= \exp\left\{-\delta\tau\,\mathfrak{P}_x(\tau+\tfrac{1}{2}\delta\tau)\right\}\mathcal{O}_x(\tau)\\ \mathfrak{P}_x(\tau+\delta\tau) &= \mathfrak{P}_{x,\mu}(\tau+\tfrac{1}{2}\delta\tau) + \tfrac{1}{2}\delta\tau\,\dot{\mathfrak{P}}_x(\tau+\delta\tau)\,.\end{aligned} \tag{B10}$$

[1] K. G. Wilson, Rev. Mod. Phys. **47**, 773 (1975).
[2] C. Wetterich, Physics Letters B **301**, 90 (1993).
[3] S. Hawking and W. Israel, eds., *General Relativity, an Einstein Centenary Survey* (Cambridge University Press, Cambridge, 1979).
[4] M. Niedermaier and M. Reuter, Living Reviews in Relativity **9** (2006).
[5] M. Reuter and F. Saueressig, Phys. Rev. D **65**, 065016 (2002).
[6] D. Benedetti, P. F. Machado, and F. Saueressig, Mod.Phys.Lett. **A24**, 2233 (2009), arXiv:0901.2984 [hep-th].
[7] D. F. Litim, Phil.Trans.Roy.Soc.Lond. **A369**, 2759 (2011), arXiv:1102.4624 [hep-th].
[8] M. Lüscher, P. Weisz, and U. Wolff, Nucl. Phys. B **359**, 221 (1991).
[9] A. Tröster, Computer Physics Communications **182**, 1837 (2011).
[10] A. Hasenfratz, P. Hasenfratz, U. Heller, and F. Karsch, Physics Letters B **140**, 76 (1984).
[11] A. Hasenfratz and A. Margaritis, Phys.Lett. **B148**, 129 (1984).
[12] S.-K. Ma, Phys. Rev. Lett. **37**, 461 (1976).
[13] C. Lang, Nucl.Phys. **B265**, 630 (1986).
[14] S. Catterall, L. Del Debbio, J. Giedt, and L. Keegan, Phys. Rev. **D85**, 094501 (2012), arXiv:1108.3794 [hep-ph].
[15] W. Bock and J. Kuti, Physics Letters B **367**, 242 (1996).
[16] S. H. Shenker and J. Tobochnik, Phys. Rev. B **22**, 4462 (1980).
[17] M. Creutz, A. Gocksch, M. Ogilvie, and M. Okawa, Phys. Rev. Lett. **53**, 875 (1984).
[18] M. Hasenbusch, K. Pinn, and C. Wieczerkowski, Nucl. Phys.Proc.Suppl. **42**, 808 (1995), arXiv:hep-lat/9411043 [hep-lat].
[19] C. Wozar, T. Kastner, B. H. Wellegehausen, A. Wipf, and T. Heinzl, PoS **LATTICE2008**, 257 (2008), arXiv:0808.4046 [hep-lat].
[20] M. Campostrini, M. Hasenbusch, A. Pelissetto, and E. Vicari, Phys. Rev. **B74**, 144506 (2006), arXiv:cond-mat/0605083 [cond-mat].
[21] J. Gasser and H. Leutwyler, Annals of Physics **158**, 142 (1984).
[22] A.M. and Polyakov, Physics Letters B **59**, 79 (1975).
[23] E. Brézin and J. Zinn-Justin, Phys. Rev. Lett. **36**, 691 (1976).
[24] W. A. Bardeen, B. W. Lee, and R. E. Shrock, Phys. Rev. D **14**, 985 (1976).
[25] I.Ya and Aref'eva, Annals of Physics **117**, 393 (1979).
[26] A. Codello and R. Percacci, Physics Letters B **672**, 280 (2009).
[27] R. Flore, A. Wipf, and O. Zanusso, Phys. Rev. **D87**, 065019 (2013), arXiv:1207.4499 [hep-th].
[28] D. Koerner, B. H. Wellegehausen, and A. Wipf, (2013), arXiv:1310.8202 [hep-lat].
[29] P. Butera and M. Comi, Phys. Rev. B **56**, 8212 (1997).
[30] M. Campostrini, M. Hasenbusch, A. Pelissetto, P. Rossi, and E. Vicari, Phys. Rev. **B65**, 144520 (2002), arXiv:cond-mat/0110336 [cond-mat].
[31] S. Antonenko and A. Sokolov, Phys. Rev. **E51**, 1894 (1995), arXiv:hep-th/9803264 [hep-th].
[32] K. Chen, A. M. Ferrenberg, and D. Landau, Phys. Rev. **B48**, 3249 (1993).
[33] L. P. Kadanoff, Physics 2 , 263 (1966).
[34] J. E. Hirsch and S. H. Shenker, Phys. Rev. B **27**, 1736 (1983).
[35] O. Bohr, B. Schaefer, and J. Wambach, Int.J.Mod.Phys. **A16**, 3823 (2001), arXiv:hep-ph/0007098 [hep-ph].
[36] J. Zinn-Justin, *Quantum Field Theory and Critical Phenomena*, 3rd ed. (Clarendon Press, 1996).
[37] H. Ballesteros, L. Fernández, V. Martín-Mayor, and A. M. Sudupe, Physics Letters B **387**, 125 (1996).
[38] A. Pelissetto and E. Vicari, Physics Reports **368**, 549 (2002).
[39] A. Wipf, Lect. Notes Phys. **864** (2013), 10.1007/978-3-642-33105-3.
[40] Y. Okabe and M. Oku, Prog.Theor.Phys. **60**, 1287 (1978).
[41] H. Gies and L. Janssen, Phys. Rev. **D82**, 085018 (2010), arXiv:1006.3747 [hep-th].
[42] J. Ambjorn, J. Jurkiewicz, and R. Loll, Nucl. Phys. **B610**, 347 (2001), arXiv:hep-th/0105267 [hep-th].
[43] J. Ambjorn, A. Goerlich, J. Jurkiewicz, and R. Loll, (2013), arXiv:1302.2173 [hep-th].
[44] B. H. Wellegehausen, A. Wipf, and C. Wozar, Phys.Rev. **D83**, 114502 (2011), arXiv:1102.1900 [hep-lat].